Journal of Materials Chemistry A

Single-ion-conducting polymer electrolytes based upon borate-chain step-growth polymers.

Journal:	*Journal of Materials Chemistry A*
Manuscript ID	TA-ART-10-2024-007236.R1
Article Type:	Paper
Date Submitted by the Author:	14-Jan-2025
Complete List of Authors:	Van Vliet, Megan; Temple University, Chemistry Wunder, Stephanie; Temple University, Chemistry Zdilla, Michael; Temple University, Chemistry

ARTICLE

Single-ion-conducting polymer electrolytes based upon borate-chain step-growth polymers.

Received 00th January 20xx,
Accepted 00th January 20xx

DOI: 10.1039/x0xx00000x

Megan M. Van Vliet,[a] Stephanie L. Wunder,*[a] and Michael J. Zdilla*[a]

Lithium salts of anionic polymers comprising internal anionic, fully saturated boron atoms are presented as single-ion-conducting polymer electrolytes. The linear linkage of BH_2^+ units by linear, bidentate *p*-catecolate, benzene-1,4-bis(thiolate), and 1,4-phenylenedimethanide is achieved by the reaction of the borate precursor $BH_2Cl(SMe_2)$ with the dilithiated substrates. These reactions give linear anionic polymers of the formula $Li[–X–C_6H_4–X–BH_2–]_n^{n-}$ (X = O, S, CH_2). A structural model compound is prepared by reaction of the lithium catecholate with triphenylboron to give the monomeic, unlinked model compound $Li_2[Ph_3B\text{-}O\text{-}C_6H_4\text{-}O\text{-}BPh_3]$, which is characterized by X-ray crystallography. In the case of the catecholate-based polymer, addition of lithium benzene-1,3,5-tris(olate) as acrosslinking agent provides a means of stiffening the polymer material. Characterization and ionic conductivity properties are described.

Introduction

Improvements to safety and performance of lithium-ion batteries (LIB) depends upon improvement of component materials to increase energy density, improve power, and mitigate safety concerns. While energy density and capacity improvements require discovery and/or implementation of new electrodes, power and safety improvements will most likely come from improvement in electrolyte technology. Battery electrolytes are typically liquids dispersed in a porous separator between the anode and cathode, and provide a medium for migration of Li^+ between the electrodes during charge and discharge of the battery. State of the art LIB technology relies on liquid organic carbonates, which offer high ionic conductivity, permitting high-current charge and discharge, and therefore, high power LIBs. However, the high performance comes at the cost of safety, since liquid electrolytes permit and can even facilitate growth of Li dendrites during charge cycles, which over time can span the separator, and short the battery. Such a battery short can lead to resistive heating that can rupture the battery casing and, combined with organic carbonates high carbon and oxygen content, can lead to explosion and fire when the cell reaches sufficiently high temperature.

To improve the safety of LIB's solid electrolytes are a target of the industry, since solids are less flammable, unlikely to be explosive, and could provide some mechanical toughness to resist dendrite growth. However, to replace current electrolytes, these need to be highly conductive, electrochemically stable, and compatible with the electrodes (meaning that if they react with the electrode(s), they form a protective solid-electrolyte interphase (SEI) layer at the interface that prevents continued electrolyte-electrode reaction and degradation, but still permit the passage of Li^+ through the SEI). In addition, low cost and easy processability using current manufacturing technology is crucial for commercial implementation of any new materials. One final opportunity for improvement would be the maximization of lithium-ion transport number, t_{Li+}, the fraction of ionic current carried by lithium ions. In current state of the art electrolyte technology, t_{Li+} <0.5, meaning most current is carried by the electrochemically inactive counterions; this leads to cell polarization which may further promote dendrite growth.

Classes of solid electrolytes that have been explored as candidates include ceramic[1, 2] and polymer[3-6] electrolytes (the two most common classes) and solvate cocrystal electrolytes pioneered by our group.[7-10] Ceramic electrolytes offer excellent conductivity and are single-ion conductors (SIC) with $t_{Li+} \approx 1$ due to an immobile anionic lattice,[1, 2] but are brittle, electrochemically incompatible with high-energy electrodes, and require high-temperature sintering to create a contiguous conducting network. Solvate cocrystals have emerged as a new class of soft electrolytes with conductivities typically better than polymer electrolytes, but not as high as ceramics. However, they show improved t_{Li+} over polymer and liquid electrolytes, and good electrode compatibility. Polymer electrolytes, typically based on polyethylene oxide (PEO) typically have poor conductivity (though they may be improved using additives or mixed-phases[11-21]), and poor t_{Li+}, but have good electrode stability and good mechanical properties and interfaces. Major improvements in polymer electrolytes would come from 1) improvement of conductivity, and 2) increases in t_{Li+} toward SIC materials.

[a] *Department of Chemistry, Temple University, 1901 N. 13th St., Philadelphia, PA 19122*

Supplementary Information available: FTIR, NMR, GPC, DSC, TGA, and electrochemical data. Crystal data for compound 3-M are available from the CCDC under deposition numbers 2380950-2380951, or as supporting files (CIF).

One approach has been to explore the use of borate decorated polymers or polymeric borate esters as solid lithium electrolyte materials.[22-30] Borate-based SICs are of interest since anionic boron charge-balances Li^+ but possess either delocalized lone pairs that bind Li^+ weakly. Such polymers retain the anionic charge directly on the polymer backbone, improving t_{Li+}, but whose conductivity may suffer from the inclusion of lithiophlilic oxygen atoms. Very little research on oxygen-free borate containing polymers exists. One advance is from the Long group, who prepared covalent networks containing tetraarylborate functionalities, which showed good conductivities and single-ion conducting behavior,[31, 32] but to our knowledge, there are no other examples. Such polymers possess anionic charge on boron, but feature no nearby lone pairs for Li^+ attachment.

In this report, we describe an approach to polymer electrolytes involving the linkage of lithiated organic linkers by BH_2 units by step-growth polymerization. We explore the linkage of dianionic *p*-disubstituted benzenes by BH_2^+ units to give lithiated anionic polymers with internalized $BH_2X_2^-$ units (X = O, S, CH_2). Their characterization and conductivity properties are discussed.

Experimental

General

Thermal gravimetric analysis (TGA) was conducted on a TA Instrument Hi-Res TGA 2950 from room temperature to 800°C at a ramp rate of 10°C/min under a nitrogen blanket, with samples ranging from 5-10mg, unless otherwise noted. Samples that were only vacuum dried showed residual THF solvent loss prior to 60°C. Subsequently, most samples were heated and vacuum dried between 60-70°C to remove residual THF for a minimum of two hours. The heat and dry method improved the temperature stability window of the samples for temperature dependent testing.

Differential scanning calorimetry (DSC) was conducted on a TA Instruments 2950 DSC in hermetically sealed Tzero Aluminum Pans in temperature ranges of -100°C to below initial degradation temperatures established from TGA analysis, at a ramp rate of 10°C/min under a nitrogen blanket, with samples in the range of 5-10mg, unless otherwise noted.

Attenuated total reflection (ATR) Fourier Transform Infrared Spectroscopy (FTIR) was conducted on a Thermo Scientific Nicolet iS5 iD5-ATR instrument. The experimental parameters use single-beam backgrounds, and 4 scans at $4cm^{-1}$ resolution from the range of $4000\text{-}600cm^{-1}$.

Gel permeation chromatography (GPC) was performed on a Shimadzu GPC with 1µL sample injections, and with acetone mobile phase at a flow rate of 1 $mL{\cdot}min^{-1}$, and with three Polymer Laboratories columns in series: PolarGel-M, PolarGel-M and PolarGel-L (300 x 7.5 mm) with 8 µm particle size and a refractive index detector. All sample solutions were on the mg/L scale.

Nuclear Magnetic Resonance (NMR) Spectroscopy was performed on a Bruker AV-III 500 MHz NMR spectrometer. Default experimental parameters are used for 1H and 11B experiments, with scans typically being 128 and 256 scans respectively. Typical samples were 1-5mg and dissolved in 1 mL of deuterated dimethylsulfoxide (DMSO).

Electrochemical impedance spectroscopy (EIS) was conducted using a Gamry Interface 1000 potentiostat/galvanostat/ZRA in the frequency range of 0.1-1MHz in temperature ranges specific to the thermal stability window of each sample determined by TGA. As shown in Figure 2.1, a custom electrochemical cell with a compression fitting is used to conduct the EIS measurements on the potentiostat; heating is done in a refitted GC oven to control temperature ramping. To confirm the polymers were chemically stable before and after EIS measurements at various temperatures, FTIR was used to check for signature chemical shifts. The bulk conductivity of samples was calculated by fitting to an equivalent electrical circuit (See SI).

Synthesis

All reactions are performed in an Argon atmosphere in an MBraun glove box unless otherwise noted. *p*-Catechol, phloroglucinol, *p*-dithiobenzene, *p*-dimethylbenzene lithium bis(trimethylsilyl)amide, chloroborane methylsulfide complex, triphenylborane were obtained from Sigma-Alrich and usedas received. Anhydrous solvents of THF, DMF, and diethyl ether are distilled from sodium benzophenone ketyl. Pentane was obtained from a PureSolv solvent purification system. All solvents were further degassed under vacuum before use. For polymeric materials, due to precipitation of monomeric species as polymers, yields were large; quantitative plus the weight of intercalated solvents.

Li_2[Ph3B-O-C6H4-O-BPh_2]·4 THF (model compound 3-M)

p-Catechol (1,4-benzenediol) (0.0050 g, 0.045 mmol) was dissolved in 10 mL THF and lithium bis(trimethylsilyl)amide (0.0150 g, 0.090 mmol) was added with stirring in a 25 mL vial. To the stirred cloudy solution, triphenylborane (0.0220 g, 0.090 mmol) was added and the solution became clear. Single crystals were grown through the use of a double-vial vapor diffusion apparatus with the THF solution and pentane as the precipitant. Unit cell: monoclinic *P*, a = 9.9479(4), b = 10.2280(5), c = 24.8303(11), β = 90.770(1)°, V = 2526.2(2).

The compound was also crystalized from benzene/pentane by vapor diffusion, to give a di-benzene solvate: Li_2[Ph3B-O-C6H4-O-BPh_2]·4 THF·2 C_6H_6. Unit cell: a = 11.2628(17), b = 13.699(2), c = 20.426(3), α = 98.899(4)°, β = 104.077(4)°, γ = 92.733(4)°, V = 3008.1(8)

Li[O-C_6H_4-O-BH_2-]$_n$ (catecholate-borate polymer 3-O)

Method A, Mixed Synthesis: Catechol [1,4-benzenediol] (0.5055 g, 4.99 mmol) was dissolved in 10 mL THF and lithium bis(trimethylsilyl)amide (1.6733 g, 9.99 mmol) was added with stirring in a 25 mL vial. This was stirred for a minimum of 30 minutes and then gravity filtered to isolate a clear to clear-yellow solution of lithiated catechol. To a stirred solution, chloroborane methylsulfide complex (1.20 mL, 10.3 mmol) was

added by dropwise addition to give an immediate exothermic reaction and the resulting opaque white precipitate agglomerate was left to stir for a minimum of 30 minutes. The solution was vacuum dried to remove THF, the residual solid was rinsed with 10 mL THF, and vacuum dried for a minimum of 2 hours at 60°C to 70°C, unless otherwise noted. ^{1}HNMR (500 MHz, DMSO-d_6): δ (ppm) 7.21, 5.21, 3.37, 2.90, 2.50, 1.76, 1.30. ^{11}B NMR (500 MHz, DMSO-d_6): δ (ppm) 20.91, 1.39, -6.48, and -13.36.

Note: When catechol borohydride polymer is left open to air, the polymer absorbs water as confirmed both visually by a swelling volume change and spectrally by FTIR with a broadening peak in the 3000 cm^{-1} region which indicates an alcohol functional group.

***Method B, Layered Synthesis*.** Chloroborane methylsulfide complex (1.20 mL, 10.3 mmol) was placed in a 25 mL vial and layered with a 0.499M solution of lithiated catechol (10.00 mL, 4.99 mmol) and left unperturbed overnight, where the opaque white precipitate formed in the interphase layer. The solution was vacuum dried to remove THF, the residual solid was rinsed with 10 mL THF, and vacuum dried for a minimum of 2 hours at 60°C to 70°C.

***Method C, Heated Synthesis*:** The 0.499M solution of lithiated catechol (10.00 mL, 4.99 mmol) was placed in a 25 mL vial and sealed with a septum. The solution was heated to 60°C with stirring, and chloroborane methylsulfide complex (1.20 mL, 10.3 mmol) was added by dropwise addition to give an immediate exothermic reaction and the resulting opaque white precipitate agglomerate was left to stir for a minimum of 30 minutes. The solution was vacuum dried to remove THF, the residual solid was rinsed with 10 mL THF, and vacuum dried for a minimum of 2 hours at 60°C to 70°C.

$Li_3[(O_3C_6H_3)_2(BH_2)_3]_n$ (branched Phloroglucinol-borate polymer 4-O)

Phloroglucinol [1,3,5-trihydroxybenzene] (0.5000 g, 3.96 mmol) was dissolved in 10 mL THF and lithium bis(trimethylsilyl)amide (1.9912 g, 11.9 mmol) was added with stirring in a 25 mL vial. This was stirred for a minimum of 30 minutes and then gravity filtered to isolate a clear to clear yellow solution of lithiated phloroglucinol. To a stirred solution, chloroborane methylsulfide complex (1.30 mL, 12.4 mmol) was added by dropwise addition to give an immediate exothermic reaction and the resulting opaque white precipitate agglomerate was left to stir for a minimum of 30 minutes. The solution was vacuum dried to remove THF, the residual solid was rinsed with 10 mL THF, and vacuum dried for a minimum of 2 hours at 60°C to 70°C.

$Li[S\text{-}C_6H_4\text{-}CH_2\text{-}S]_n$ (dithiobenzene-borate polymer 3-S)

Dithiobenzene (0.5000 g, 3.52 mmol) was dissolved in 10 mL THF and lithium bis(trimethylsilyl)amide (1.176 g, 7.04 mmol) was added with stirring in a 25 mL vial. This was stirred for a minimum of 30 minutes and then gravity filtered to isolate a clear yellow solution of lithiated dithiobenzene. To a stirred solution, chloroborane methylsulfide complex (0.8 mL, 7.67 mmol) was added by dropwise addition to give an immediate reaction and the resulting opaque white precipitate was left to stir for a minimum of 30 minutes. The solution was vacuum dried for a minimum of 2 hours at 60°C. The synthesized polymer was an opaque white to grayish-white color and tacky solid. ^{1}H NMR (500 MHz, DMSO-d_6): δ (ppm) 6.38, 5.32, 4.61, 4.47, 3.41, 2.85, 1.84, 3.64, 1.74, 3.33, 2.50, 1.52, 1.29, 0.01. ^{11}B-NMR (500 MHz, DMSO-d_6): δ (ppm) 24.59, 21.84, 1.43, -8.25.

$Li[CH_2\text{-}C_6H_4\text{-}CH_2\text{-}BH_2\text{-}]_n$ (xylene-borate polymer 3-CH_2)

The *p*-xylene lithiation reaction was reported by Bates et al.[20] To a pressure flask stirring 20 mL pentane, potassium tert-butoxide (0.8000 g, 7.17mmol), para-dimethylbenzene (0.40 mL, 3.33 mmol) and 2.5 M n-BuLi in hexanes (3.00 mL, 7.50 mmol) are added in sequential order. Almost immediately upon addition of n-BuLi forms a red precipitate. The solution was allowed to stir for several hours before filtering, rinsing the precipitate with pentane and vacuum dried. An aliquot of the resulting precipitate (0.0120 g, 0.12 mmol) was stirred in 2 mL pentane and quenched with chlorotrimethylsilane (0.30 mL, 0.24 mmol) where the red suspension color disappears to white. The quenched product is washed with deionized water, and the pentane layer is separated, dried, and the residue is dissolved into $CDCl_3$ for NMR analysis, see Appendix A.6. Lithiated dimethylbenzene (0.1000 g, 0.85mmol) was stirred in 10 mL THF, and chloroborane methylsulfide complex (0.2 mL, 1.92 mmol) was added by dropwise addition to give an immediate reaction and the resulting opaque white precipitate was left to stir for a minimum of 30 minutes. The solution was vacuum dried for a minimum of 2 hours at 60°C. The synthesized polymer was an opaque white tacky solid. ^{1}H NMR (500 MHz, DMSO-d_6): δ (ppm) 7.36, 7.07, 6.54, 5.33, 4.61, 4.47, 3.63, 3.41, 3.33 2.86, 2.50, 1.84, 1.75, 1.51, 1.32, 1.23, 1.09, 0.85, 0.18, 1.32. ^{11}B-NMR (500 MHz, DMSO-d_6): δ (ppm) 20.93, 1.45, -5.10.

Results and Discussion

Synthesis and characterization.

The basic synthetic approach involves step-growth polymerization by the reaction of the zwitterionic adduct of chloroborane and dimethylsulfide (**1**) with dilithiated *p*-substituted benzene (**2-X_2**). The reaction results in the replacement of the Cl atom by a substituted phenyl, aided by elimination of LiCl, which precipitates. The weakly-bound dimethylsulfide is removed by replacement with the stronger second B-X bond, resulting in a polymer with one anionic borate atom per unit, charge balanced by one Li ion (**3-X** eq. 1).

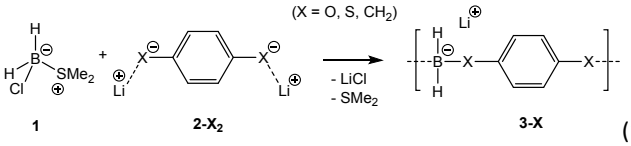

(1)

Catecholate-based polymers (3-O)

In the case where lithium catecholate (X = O) is used, the consistency of the resulting polymer, $Li[BH_2\text{-}O\text{-}C_6H_4\text{-}O]_n$ (**3-O**) ranged from a sticky, viscous fluid to a solid with the consistency of hard candy. Due to the nature of step-growth polymerization, where the two monomeric precursors "take turns" attaching in an alternating fashion, reproducing the average molecular weight can be challenging if the stoichiometries are not equal during the reaction synthesis, with greater excess reagents leading to shorter polymers, and more exact 1:1 stoichiometries giving larger polymers. The polymer consistency will be crucial for the collection of electrochemical data on the samples; the harder samples perform better due to their rigidity, which prevents short circuiting of the cell (vide infra).

We explored the preparation of these polymers using four different reaction conditions: 1) room temperature mixing and stirring of the two reagents in tetrahydrofuran (THF); 2) room temperature mixing and stirring of the two reagents in tetrahydrofuran (THF), followed by removal of THF in vacuo at elevated temperature (60°C); 3) elevated-temperature (60°C) mixing, stirring, and drying; and 4) a slow layer-diffusion of the two reagents at room temperature, gently layered such that the reaction occurs at the surface interfaces, followed by removal of THF in vacuo with heating. Analysis of polymers by FTIR demonstrates the retention of the B-H stretch and bending modes, demonstrating the retention of the borohydride moieties in the polymer following polymerization (Figure S1NMR spectroscopies support the formation of four-coordinate borate-based species (Figure S6). The proton resonances of the ^{1}H NMR spectrum shift upfield in comparison to the catechol starting material (Fig. S5), suggesting increased negative charge from the formation of the anionic polymer. In the ^{11}B NMR spectrum, the resonances for boron in the polymer have negative chemical shift, demonstrating that they are much more shielded than those of neutral boron, or even oxyborate species, which have positive chemical shifts.[33-40] Additional discussion of the NMR spectra is provided in the supporting information.

TGA of the samples is shown in Figure 1. The room-temperature-dried sample, typically stickier and more fluid, shows an initial weight loss at ~50°C. With heating and drying of the samples, they become stiffer, and this initial weight loss is extended to ~70°C, which suggests that the initial weight loss is due to residual THF solvent. The first derivative plot emphasizes that heating and drying the samples increases the temperature of the initial weight loss in comparison to the room-temperature-dried (yellow) samples from ~ 50 °C to ~ 70 °C, and that the samples do not fully decompose until above 150°C. The DSC does not show any remarkable features between the temperatures of 30 °C and -110 °C (Figure S10).

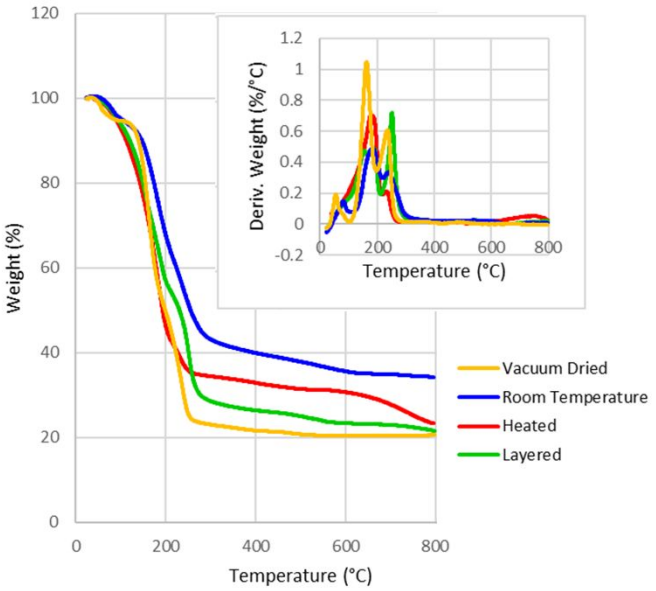

Figure 1. TGA of **3-O** from various reaction conditions, Inset: First derivative plots.

Gel permeation chromatography (GPC) was performed to assess the molecular weight of **3-O** based on the synthetic method used to prepare the polymer. While the polymers were fully soluble in DMSO, instrumental limitations prevented DMSO-based samples to be analyzed by GPC, so acetone was used, though in some cases samples did not fully dissolve. The general trend shows that heated samples form higher molecular weights (longer chains) than room-temperature treatments, and that the layered-phase synthesis gives the largest chains (Figure S9, Table S3). Polymer lengths ranged from about 20-30 units in length. These results are consistent with the observed consistency of the materials.

Catecholate-based polymers: model compound 3-M

Since polymer **3-O** is a challenge to structurally characterize, we prepared a model segment of the repeating unit by replacing the bridging BH_2 precursor **1** with two equivalents of a capping triphenylborane model. These boranes are expected to be coordinated by the aryloxide ligands of **2-O$_2$**, generating a small-molecule polymer fragment analogue, $Ph_3B\text{-}O\text{-}C_6H_4\text{-}O\text{-}BPh_2$ (**3-M**) that could be structurally characterized (eq. 2).

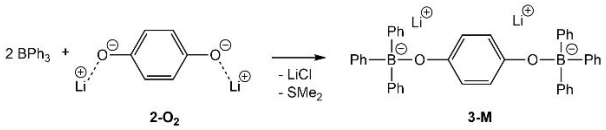

(2)

Single-crystal X-ray diffraction analysis reveals the expected structure with Li^+ ions weakly coordinated to the borate oxygen atom and THF with Li···O contacts in the range of 1.87-1.90 Å. As expected, the Li^+ is not associated with the formally anionic boron atom, but with the lone pair of the catecholate oxygen atom, which is a relatively poor Lewis base due to resonance delocalization of the oxygen lone pair into the aryl ring.

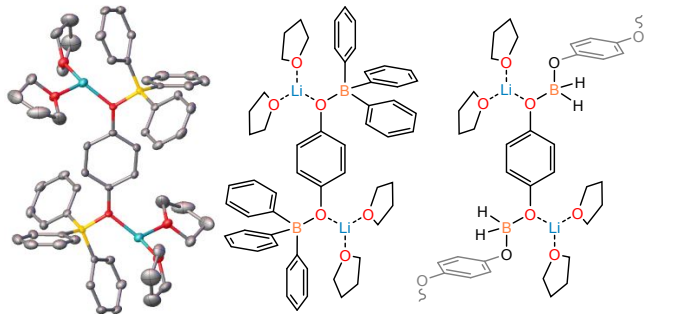

Figure 2. Left: Single-crystal X-ray structure of **3-M** with ellipsoids set at 50% probability level. Benzene solvate molecules, 2nd component of disordered THF, and hydrogen atoms omitted for clarity. Center: Lewis structure of **3-M**. Right: Hypothetical structure of a fragment of polymer **3-O** based on analogy to **3-M**.

Phloroglucinol-based polymer 4-O

For comparison to the bifunctional catecholate precursor, we explored the use of 1,3,5-trihydroxybenzene (phlorogluciol) as a precursor for SIC polymers. Unlike catecholate, which is expected to form linear polymers, phloroglucinolate would be expected to form branched polymers or covalent frameworks (eq 2).

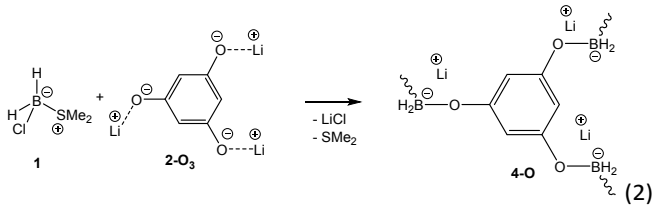

(2)

FTIR spectroscopy on polymer **4-O** (Figure S2) shows the expected appearance of B-H vibrations in the polymer product **3-O**. Polymer **4-O**, exhibits a similar range of stiffnesses to **3-O**, though being presumably branched, somewhat improved toughness, as evidenced by the firmer texture and higher decomposition temperatures based on TGA (See Figure S11). The stability of material **4-O** shows similar trends as **3-O** as a function of synthetic method, with room temperature preparations being the least robust, and the layer-diffusion based synthesis being the most robust. GPC reflects these trends as well, though the GPC calibration does not account for branching volume, and since the phloroglucinol is expected to be branched and the catechol to be linear, it is not possible to make a direct comparison by MW. Thus, the phloroglucinol molecular weights should be considered lower-bound estimates.

Benzene-1,4-dithiolate-based polymer (3-S)

The catechol and phloroglucinol based polymers bind lithium via the borate ether oxygen atom based upon model compound **3-M** shown in Figure 2. Based upon Pearson Hard-Soft-Acid-Base (HSAB) theory, oxygen generally has a high affinity for lithium since ether oxygen and lithium ions are both hard (small, charge dense, non-polarizable). While the neighbouring phenyl group does help to polarize the lone pair into the ring, making these oxygen atoms softer, the choice of other binding groups could further weaken the interaction with lithium, facilitating ionic mobility. The larger and more polarizable sulfur donors are a softer alternative to oxygen. Polymers were prepared using an identical approach as that shown in Equation 1, using lithium 1,4-dithiolate as the Lewis basic monomer.

TGA (Figure S12) indicates that the dithiobenzene borohydride polymer **3-S** exhibits an improved thermal stability upwards of >90°C (dithiobenzene itself has a melting point of 92-97°C as reported by Sigma-Aldrich), in comparison **3-O**, which began decomposing at 60°C. Remarkably at ~130°C there was less than 2.5 percent weight loss of the **3-S**, whereas **3-O** had lost 7% of its mass by this temperature. There was also less of an initial weight loss in the thiol compound ascribed to desolvation of THF, which may be due to the increased drying time (see Experimental section).

The FTIR spectra of 3-S is compared with other 3-X samples in Figure S4 and summarized in Table SX. The 3-S compound generally exhibit the same features, suggesting similar structures. As shown in Figure S2, there are several new strong-intensity peaks related to the dithiobenzene functionality: sulfur-hydrogen, carbon-sulfur or carbon-sulfur double bonds at 2545cm-1, 650cm-1 and 3440cm^{-1} wavenumbers respectively. The small sharp peak at 3400cm^{-1} may be due to S-BH_2 bond vibrations. The broadening of the peak at 2400cm^{-1} is most likely due to the BH_2 signature peak overlapping with the sulfur linker at 2500cm^{-1}. Furthermore, peak intensity increases in the fingerprint region are most likely due to increased C-S character for the 710-550cm^{-1} signals.

The formation of four-coordinate boron in **3-S** is confirmed by the upfield shift of the aromatic protons (δ 7.16 to δ 6.38) of the ^{1}H NMR spectrum (Figure S7). Also shown in this figure, the ^{11}B-NMR spectrum exhibits the expected upfield shift for a tetravalent, anionic boron atom.

***p*-xylene-based polymer (3-CH_2)**

As a final variation, we prepared a version of the linear borate polymer with lithiated xylene, which upon forming C-B covalent bonds in polymer **3-CH_2**, would result in an anionic polymer system with no lone pair electrons. Unlike the lithium association shown in model **3-M**, where lithium binds to the oxygen (or in the case of **3-S**, the sulfur) atom, there is no lone pair on the methylene group of **3-CH_2**, and so the geometry of the salt is less clear, and we hypothesized that this Li^+ would be bound more weakly, and thus be more mobile, giving higher conductivity. (This turns out not to be the case; *vide infra*).

The dimethylbenzene borohydride polymer **3-CH_2** also had higher thermal stability than **3-O**. At 70°C only 1% weight loss occurred, and at 90°C only 3%. As the boiling point for parent *p*-xylene is approached (~138°C) the weight loss approaches only 6%. The TGA plot shows distinct regions for polymerized vs. monomeric species, suggesting a good degree of polymerization.

As shown in Figure S4 and Table S2, and as in the case of the other polymers, the FTIR spectrum exhibits many common

features, suggesting analogous structure. There are fewer differences between the spectra of **3-O** and **3-CH$_2$**, presumably due to the lower-polarity, hydrocarbon character of **3-CH$_2$**, but distinctive B-H peaks as well as B-C peaks are present in regions frequently found to overlap at typical B-O bond wavenumbers (See Table S2). The ^{1}H-NMR and ^{11}B-NMR spectra shown in Figure S7 show the similar expected upfield shifts associated with tetravalent borate formation.

Conductivity measurements

Conductivity was measured using electrochemical impedance spectroscopy. Nyquist plots were fit to equivalent circuit models to extract bulk conductivity (See Supporting Information). In Figure 3, comparisons of the temperature-dependent bulk ionic conductivity of the catechol- and phloroglucinol -based systems are shown. Figure 3 shows that the application of heat and vacuum drying of the polymer samples not only helps improve the thermal stability window of the catechol borohydride polymers by removing excess solvents (see Figure 1, S11, S12), it seems to improve the ionic conductivity. Without vacuum drying, the THF may act as a HSAB "hard" donor and bind the Li ions, limiting their contribution to the overall ionic conductivity of the polymer. The highest ionic conductivity measured for the unheated synthesis of **3-O** was at 50°C and was only 3.7 x 10^{-7} S·cm^{-1} . In contrast, at 60°C the heated synthesis of **3-O** exhibited a conductivity of 2.2 x 10^{-5} S·cm^{-1} for the heated and vacuum dried catechol borohydride polymer, competitive with PEG-based polymers, but with presumed single-ion conductivity. For this reason, the heated synthesis and vacuum-dried workup was used for all subsequent materials. The phloroglucinol-based polymer **4-O** showed lower conductivity than **3-O**: 1.1 x 10^{-7} S·cm^{-1} at 70°C.

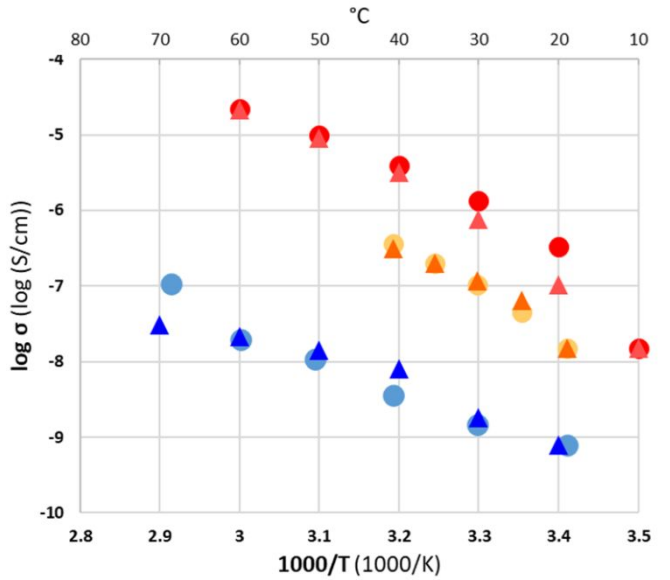

Figure 3. Temperature dependent conductivity of **3-O** and **4-O**. ● : **3-O**, unheated synthesis, cooling sweep, ▲ : **3-O**, unheated synthesis, warming sweep, ● : **3-O**, heated synthesis, cooling sweep, ▲ : **3-O**, heated synthesis, warming sweep, ● : **4-O**, cooling sweep, ▲ : **4-O**, warming sweep.

As shown in Figure 3, the data approximately follow the Arrhenius law. The slight curvature exhibited in the plots constitute a slight deviation to Arrhenius law, and are ascribed to the amorphous structure, and the associated chain-side-motion-based mechanism of ion conductivity within the polymers themselves.[2,20] At higher temperature, the viscosity decreases and increases segmental motion so that ions can then hop between neighboring chains more favorably (as opposed to the lower temperature regions which are more ordered, and reduce the number of segmental motions and in turn the ion mobility.[20–23]) Activation energies for all the polymers are similar, ranging from 110 to 125 kJ/mol (see Supporting Information for more details).

As shown in Figure 4 the conductivity data for **3-S** are slightly improved over the best samples of **3-O** at both high and low temperature, with an ionic conductivity value of 1.4 x 10^{-4} S·cm^{-1} at 60 °C, 5.1 x 10^{-8} S·cm^{-1} at 10 °C, but with a similar activation energy of 106-120 kJ/mol. The similar activation energies (slopes), but larger Arrhenius constant (vertical position) for **3-O** suggests a similar barrier to migration, but that there are more charge carriers available. This suggests that segmental motion of the polymer chain may still represent the rate limiting step for ion migration, but that more Li^{+} ions are available due to the softer nature of the sulfide donors, which are expected to interact more weakly with hard lithium ions.

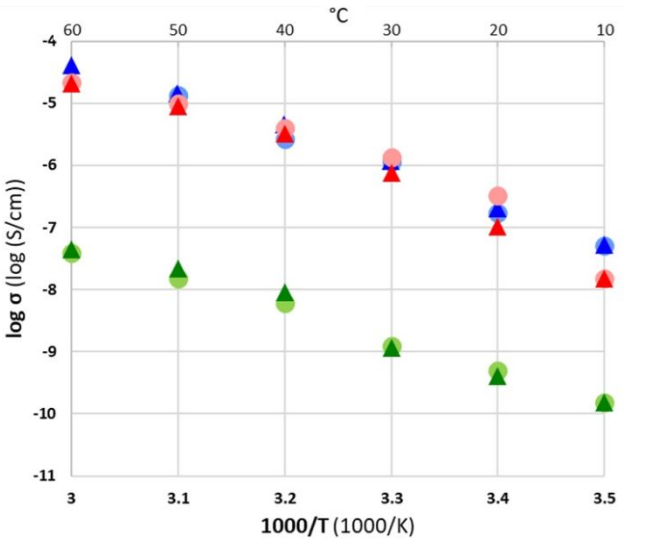

Figure 4. Temperature dependent conductivity of **3-S** and **3-O** in comparison to **3-O**. ● : **3-CH$_2$**, cooling sweep, ▲ : **3-CH$_2$**, warming sweep, ● : **3-S**, cooling sweep, ▲ : **3-S**, warming sweep, ● : **3-O**, cooling sweep, ▲ : **3-O**, warming sweep.

To our surprise the ionic conductivity of **3-CH$_2$** system was poorest. However, despite the lower Arrhenius constant, this system exhibited a lower activation energy of ~90kJ/mol (See Table SX in Supporting Information for more details). This decrease in activation energy compared to all other polymers in this study, which themselves possessed similar activation energies, suggest that the mechanism may be different for this material, and that polymer segmental motion may play less of a role in the rate limiting step. This may be due to the lack of Lewis basic lone pairs on **3-CH$_2$** in comparison to **3**-O, **3**-S, and 4-**O** (Figure 5). The lower Arrhenius constant for **3-CH$_2$** indicates that there are fewer charge carriers. This may be because in the absence of Lewis donors on **3-CH$_2$**, the compound tightly retains

THF, and that the "hard" THF donors restrict the number of mobile lithium ions.

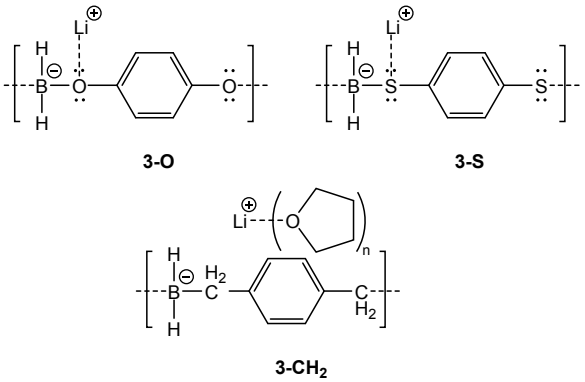

Figure 5. Lewis structures of hypothetical polymer-lithium aggregates. The polymers **3-O**, **3-S**, and **4-S** (not shown), have lone pair electrons that associate with the lithium ions, requiring polymer chain segmental motion for conductivity. Polymer **3-CH$_2$** is designed to have no lone pairs, and thus is not expected to form Lewis pairs with lithium ion. However, carrier count may be limited by coordination to THF ligands.

The conductivity values for the best performing electrolytes in this set range from 10^{-7} to 10^{-6} Scm^{-1} at room temperature, and approach 10^{-4} Scm^{-1} at elevated temperature (60°C). These are lower than the conductivities of commercial liquid electrolytes (~10^3 Scm^{-1}), but are in line with pure samples of polymer electrolytes, most of which are PEO.[41] However, those PEO based electrolytes typically have low t_{Li+} in the range of 0.2-0.3, suggesting only one fifth of the conductivity is attributable to lithium ion, whereas in the current report the anionic nature of the polymer will limit anion migration to near zero. As such, these materials show comparable conductivity to typical polymer electrolytes but with presumably higher t_{Li+}.

Despite promising conductivity for a new class of polymer electrolyte, these materials did not show good electrode stability against Li(s) or other high-energy anodes, precluding t_{Li+} measurements and cycling tests. CV results using Li(s) reference electrodes resulted in electrode fouling, and no observation of formation of a conductive SEI or Li stripping and plating. We attribute the decomposition to the selection of "benzylic" type linker atoms (adjacent to the arene ring) which exhibit weaker bonding, and can stabilize radicals during reductive decomposition via delocalization of radicals into the arene ring.

Conclusions

We describe the preparation and characterization of anionic polymers where the mobile ionic phase is only Li$^+$. Conductivity measurements reveal a similar activation energy for oxygen- and sulfur-containing polymers, with the mechanism of conduction attributed to the common segmental chain motion of the polymer. The xylene-based polymer, which contains no heteroatom lone pairs, shows a reduced activation barrier consistent with lithium ions dissociated from the anionic backbone, but with lower overall carrier number. However, these first generation samples showed poor electrode stability, attributed to decomposition at the redox-sensitive "benzylic" sites which have weak bonds, and which stabilize radicals during reductive decomposition. Future work will focus on polymers without lone pairs (for higher Li mobility), and short aliphatic linkers, with the goal to increase flexibility, and shorten the linker between the anionic borate sites and improve redox stability. We hypothesize these changes will increase lithium mobility by making polymer backbones more flexible and having a higher density of Li$^+$ ions, and will improve electrochemical stability by featuring much more robust bonding networks.

Author contributions

MJZ – Conceptualization, funding acquisition, project administration, supervision, writing—original draft

SLW – Conceptualization, resources, supervision, writing—review and editing

MV – Investigation, methodology, validation, writing—review and editing

Conflicts of interest

There are no conflicts to declare.

Data availability

Crystal data for compound **3-M** are available from the CCDC under deposition numbers 2380950-2380951. Additional data are provided in the Supporting Information, or by request from the authors.

Acknowledgements

Support of this work from NSF under award DMR-330705 is gratefully acknowledged. The authors gratefully acknowledge Thomas Boller and Laura Sonnenberg for assistance with GPC measurements.

Notes and references

1. Z. Gao, H. Sun, L. Fu, F. Ye, Y. Zhang, W. Luo and Y. Huang, *Adv. Mater.*, 2018, **30**, 1705702.
2. J. Lau, R. H. DeBlock, D. M. Butts, D. S. Ashby, C. S. Choi and B. S. Dunn, *Advanced Energy Materials*, 2018, **8**, 1800933.
3. G. S. MacGlashan, Y. G. Andreev and P. G. Bruce, *Nature*, 1999, **398**, 792-794.
4. Z. Gadjourova, Y. G. Andreev, D. P. Tunstall and P. G. Bruce, *Nature*, 2001, **412**, 520-523.
5. C. H. Zhang, D. Ainsworth, Y. G. Andreev and P. G. Bruce, *J. Am. Chem. Soc.*, 2007, **129**, 8700-8701.
6. Z. Stoeva, I. Martin-Litas, E. Staunton, Y. G. Andreev and P. G. Bruce, *J. Am. Chem. Soc.*, 2003, **125**, 4619-4626.
7. P. R. Chinnam, R. N. Clymer, A. A. Jalil, S. L. Wunder and M. J. Zdilla, *Chem. Mater.*, 2015, **27**, 5479-5482.

8. B. Fall, A. Jalil, M. Gau, S. Chereddy, M. J. Zdilla, S. L. Wunder and P. R. Chinnam, *Ionics*, 2017, DOI: 10.1007/s11581-017-2206-7.
9. P. Prakash, J. Aguirre, M. M. Van Vliet, P. R. Chinnam, D. A. Dikin, M. J. Zdilla, S. L. Wunder and A. Venkatnathan, *Journal of Materials Chemistry A*, 2018, **6**, 4394-4404.
10. P. Prakash, B. Fall, J. Aguirre, L. A. Sonnenberg, P. R. Chinnam, S. Chereddy, D. A. Dikin, A. Venkatnathan, S. L. Wunder and M. J. Zdilla, *Nature Materials*, 2023, **22**, 627-635.
11. J. Yin, X. Xu, S. Jiang, H. Wu, L. Wei, Y. Li, J. He, K. Xi and Y. Gao, *Chem. Eng. J.*, 2022, **431**, 133352.
12. F. Croce, G. B. Appetecchi, L. Persi and B. Scrosati, *Nature*, 1998, **394**, 456-458.
13. F. Croce, R. Curini, A. Martinelli, L. Persi, F. Ronci, B. Scrosati and R. Caminiti, *J. Phys. Chem. B*, 1999, **103**, 10632-10638.
14. A. M. Stephan, T. P. Kumar, M. A. Kulandainathan and N. A. Lakshmi, *J. Phys. Chem. B*, 2009, **113**, 1963-1971.
15. N. F. Uvarov, *J. Solid State Electrochem.*, 2011, **15**, 367-389.
16. E. Tsuchida, N. Kobayashi and H. Ohno, *Macromolecules*, 1988, **21**, 96-100.
17. S. W. Ryu, P. E. Trapa, S. C. Olugebefola, J. A. Gonzalez-Leon, D. R. Sadoway and A. M. Mayes, *J. Electrochem. Soc.*, 2005, **152**, A158-A163.
18. C. H. Park, Y. K. Sun and D. W. Kim, *Electrochim. Acta*, 2004, **50**, 375-378.
19. P. R. Chinnam and S. L. Wunder, *Chem. Mater.*, 2011, **23**, 5111-5121.
20. P. R. Chinnam, H. Zhang and S. L. Wunder, *Solid State Ionics*, 2013, **submitted**.
21. Y. Inokuma, S. Yoshioka, J. Ariyoshi, T. Arai, Y. Hitora, K. Takada, S. Matsunaga, K. Rissanen and M. Fujita, *Nature*, 2013, **495**, 461-466.
22. W. Xu, X.-G. Sun and C. Austen Angell, *Electrochim. Acta*, 2003, **48**, 2255-2266.
23. N. Matsumi, K. Sugai and H. Ohno, *Macromolecules*, 2003, **36**, 2321-2326.
24. M. Saito, H. Ikuta, Y. Uchimoto, M. Wakihara, S. Yokoyama, T. Yabe and M. Yamamoto, *The Journal of Physical Chemistry B*, 2003, **107**, 11608-11614.
25. M. Marzantowicz, A. Sami, K. Pożyczka, A. Chodara, D. Gładka, E. Zygadło-Monikowska and F. Krok, *Electrochim. Acta*, 2023, **469**, 143203.
26. J. Son, C. Barcha, S. Grugeon, D. Sicsic, N. Besnard, M. Courty and M. Becuwe, *Chem. Commun.*, 2023, **59**, 1066-1069.
27. K. Dai, C. Ma, Y. Feng, L. Zhou, G. Kuang, Y. Zhang, Y. Lai, X. Cui and W. Wei, *Journal of Materials Chemistry A*, 2019, **7**, 18547-18557.
28. B. Zhou, Y. Zhou, L. Lai, Z. Chen, J. Li, Y. Jiang, J. Liu, Z. Wang and Z. Xue, *ACS Applied Energy Materials*, 2021, **4**, 9582-9593.
29. G. Guzmán-González, S. Vauthier, M. Alvarez-Tirado, S. Cotte, L. Castro, A. Guéguen, N. Casado and D. Mecerreyes, *Angew. Chem. Int. Ed.*, 2022, **61**, e202114024.
30. L. Wan, X. Tan, X. Du, X. Xue, Y. Tong, D. Zhou, Y. Ling, Y. Xie and J. Zhao, *Eur. Polym. J.*, 2023, **195**, 112191.
31. J. F. Van Humbeck, M. L. Aubrey, A. Alsbaiee, R. Ameloot, G. W. Coates, W. R. Dichtel and J. R. Long, *Chemical Science*, 2015, **6**, 5499-5505.
32. D.-M. Shin, J. E. Bachman, M. K. Taylor, J. Kamcev, J. G. Park, M. E. Ziebel, E. Velasquez, N. N. Jarenwattananon, G. K. Sethi, Y. Cui and J. R. Long, *Adv. Mater.*, 2020, **32**, 1905771.
33. J. D. Odom, T. F. Moore, R. Goetze, H. Nöth and B. Wrackmeyer, *J. Organomet. Chem.*, 1979, **173**, 15-32.
34. R. A. Oliveira, R. O. Silva, G. A. Molander and P. H. Menezes, *Magn. Reson. Chem.*, 2009, **47**, 873-878.
35. G. R. Eaton, *J. Chem. Educ.*, 1969, **46**, 547.
36. D. L. Bryce, R. E. Wasylishen and M. Gee, *The Journal of Physical Chemistry A*, 2001, **105**, 3633-3640.
37. S. L. Diemer, M. Kristensen, B. Rasmussen, S. R. Beeren and M. Pittelkow, *Journal*, 2015, **16**, 21858-21872.
38. W. L. Smith, *J. Chem. Educ.*, 1977, **54**, 469.
39. B. Wrackmeyer, *Prog. Nucl. Magn. Reson. Spectrosc.*, 1979, **12**, 227-259.
40. S. Hermanek, *Chem. Rev.*, 1992, **92**, 325-362.
41. J. W. Fergus, *J. Power Sources*, 2010, **195**, 4554-4569.

Data availability statement

Crystallographic data are archived by the CCDC under deposition numbers 2380950-2380951 and are provided as supporting information. Comprehensive spectral, electrochemical, and thermal analysis data are given in the supporting information.